RSC Applied Polymers

ROYAL SOCIETY OF CHEMISTRY

PAPER

View Article Online
View Journal | View Issue

Cite this: *RSC Appl. Polym.*, 2024, **2**, 47

Aromatic polypeptide amphiphiles for drug adsorption: a new approach for drug overdose treatment†

Karoline E. Eckhart, ‡[a] Hunter B. Wood, ‡[a] Tarik A. Taoufik,‡[a] Michelle E. Wolf, [a] Dazhe J. Cao[b] and Stefanie A. Sydlik *[a]

The drug overdose epidemic in America has intensified over the past 20 years and has led to hundreds of thousands of deaths. Opioids account for most of these deaths, but overdose can be effectively reversed using naloxone, an FDA-approved medication. The rate of non-opioid drug fatalities has also risen in recent years—but unlike opioids—many of these drugs do not have specialized treatments in cases of overdose. Instead, activated charcoal is ingested to decontaminate the gastrointestinal tract before the drug is absorbed by the blood. Although activated charcoal is an effective drug adsorbent, there are many adverse side effects following respiratory and oral exposure. To address the drawbacks of this treatment, a new class of aromatic polypeptide amphiphiles (termed "KEYs") were developed to adsorb drugs from the stomach and intestines without harmful side effects. This manuscript details the rational design and synthesis of KEY polypeptide adsorbents. KEYs were evaluated against model compounds acid yellow 3 and amitriptyline in simulated biological media and compared to activated charcoal. Adsorption studies indicate that KEYs are capable of adsorbing drugs. KEYs adsorb molecules as rapidly as activated charcoal and adsorb certain compounds with comparable or higher adsorption capacity in a pH-dependent manner. This work represents a novel application of aromatic polypeptide amphiphiles as a gastrointestinal decontamination technology. Further, these studies provide insight for how future generations of polypeptide-based adsorbents can be rationally designed to selectively target and improve drug adsorption from the gastrointestinal tract.

Received 12th June 2023,
Accepted 13th September 2023

DOI: 10.1039/d3lp00082f

rsc.li/rscapplpolym

1. Introduction

The rate of drug overdose fatalities in America has steadily increased over the past 20 years.[1] Between 1999 and 2016, opioid overdose increased by 371% and accounted for the majority of the drug overdoses.[2] Importantly, the number of non-opioid drug fatalities also rose by 274% during this period. While opioid overdose can often be reversed with naloxone if treatment is initiated quickly and frequently,[3,4] many non-opioid drugs do not have effective antidotes. In some cases, the only way to treat these specific overdoses is to decontaminate the gastrointestinal tract before the drug can be absorbed by the blood. Typically, gastrointestinal decontamination is achieved by administering activated charcoal (AC) either orally or through a stomach tube, to adsorb the overdosed drug(s) from the stomach.[5]

The physical and chemical composition of AC make it an effective drug adsorbent. AC is highly porous and possesses a remarkably high surface area that is available for adsorption of drugs and other molecules.[6,7] The surface of AC is composed of a delocalized π-system that can participate in interactions with the aromatic π-electrons of an adsorbate.[6,7] AC can also adsorb compounds through hydrogen bonding and electrostatic attraction, making it an effective adsorbent through a variety of interactions.[6] Moreover, AC is an inexpensive feedstock that can be prepared from a variety of waste products[8–10] which makes it ideal for commercial use. These properties have made AC a life-saving overdose treatment, positioning it as the clinical standard for treatment of overdose from drugs including antidepressants and barbiturates.[5]

The efficacy of *in vivo* drug adsorption by AC has been thoroughly demonstrated.[11,12] Since it is not systemically

[a]*Department of Chemistry, Carnegie Mellon University, 4400 Fifth Avenue, Pittsburgh, PA, USA. E-mail: ssydlik@andrew.cmu.edu*
[b]*Department of Emergency Medicine, University of Texas Southwestern Medical Center, Dallas, TX, USA*

† Electronic supplementary information (ESI) available: Structures, synthesis protocols, characterization, and supplemental data (UV-Vis calibration curves, non-linear Langmuir isotherm fits, comparison of linear *versus* non-linear Langmuir isotherm fits, and control experiment results). See DOI: https://doi.org/10.1039/d3lp00082f

‡ These authors contributed equally.

absorbed by the body, there is also no significant toxicity associated with AC.[13] However, the administration of AC is not without risk. One of the well-documented hazards of this treatment is pulmonary aspiration of the AC, which can occur during ingestion, emesis, or as a result of ill-fitting nasogastric tubes.[14] Aspiration of AC allows activated charcoal to enter the lungs where it may lead to a variety of respiratory issues—and in severe cases—death.[15,16] Even in mild cases of AC aspiration, patients have developed acute respiratory distress syndrome,[17] persistent parenchymal disease,[17] chronic lung disease,[18] obstructive laryngitis,[19] granulomatous lung mass,[20] charcoal empyema,[21] and bronchiolitis obliterans.[22] Gastrointestinal complications may also occur as a result of treatment with AC. Isolated case reports note the formation of bowel obstructions, bezoars, and stercoliths following administration of AC, for which surgical intervention is sometimes the only solution.[23,24]

Due to these concerns, researchers have developed a variety of adsorbent materials as alternatives to AC. For example, AC has been chemically modified to prevent accumulation in the gastrointestinal tract and to increase its adsorption capacity as a strategy to lower the effective dose.[25] Researchers have also investigated the adsorption properties of other highly porous natural materials, including smectite clays, zeolites, and mesoporous silica.[26–30] Furthermore, new macromolecular systems using nanocellulose,[31–33] genomic DNA-coated substrates,[34,35] or charged block copolymers[36–38] have been developed for drug adsorption applications, particularly with the goal of preventing off-target effects of chemotherapy drugs. However, many of these macromolecular systems were not designed for or evaluated in gastrointestinal conditions, where pH and salt concentrations (which are known to influence adsorption capacity) vary widely from serum. A growing area of research explores drug delivery systems based on polypeptides. Since they model naturally occurring compounds, synthetic polypeptides are generally regarded as biocompatible and well-tolerated when introduced *in vivo*.[39–42] Polypeptides also typically to bind to specific receptors, negating adverse health effects by avoiding interactions with other parts of the body.[43]

To address the drawbacks of AC, a new class of aromatic polypeptide amphiphiles (termed "KEYs") were prepared for the purpose of adsorbing drugs from the stomach and intestines without harmful side effects. The adsorbents were rationally designed to possess K (lysine), E (glutamic acid), and Y (tyrosine) amino acid residues, hence they are named "KEYs". Existing literature includes the preparation of synthetic, zwitterionic polypeptides (*i.e.* KE polypeptides) as antifouling materials[44] and amphipathic polypeptides (*i.e.* KY polypeptides) for the purpose of drug delivery.[45] However, the preparation and evaluation of KEY polypeptides is not reported, particularly in the context of drug adsorption.

This work describes the synthesis and evaluation of KEYs as drug adsorbents and compares their performance to the clinical standard, AC. By controlling amino acid composition, KEYs are designed to participate in π–π stacking, electrostatic interactions, and hydrogen bonding to adsorb aromatic and charged drug molecules. Unlike AC, which indiscriminately adsorbs material, the adsorption capacity of the KEYs is dependent on amino acid composition, the identity of the adsorbate, and the pH of the media. Compared to activated charcoal, these characteristics afford KEYs more specificity and control over adsorption. Overall, this work provides proof of concept for the adsorption of drug compounds to polypeptides and provides insights that may improve the efficacy of future generations of polypeptide-based adsorbents.

2. Experimental

2.1 Materials

Amino acids (N_6-carbobenzyloxy-L-lysine, γ-benzyl-L-glutamate, and *O*-benzyl-L-tyrosine) and triphosgene were obtained from ChemImpex and used without further purification for the *N*-carboxyanhydride (NCA) synthesis. Solvents for synthesis (tetrahydrofuran, dimethylformamide, diethyl ether) and glacial acetic acid were obtained from Fisher Chemical. Methanol was obtained from Pharmco. Tetrahydrofuran (THF) and dimethylformamide (DMF) were dried *via* solvent still, degassed with dry N_2, and passed through a column of activated neutral alumina before use. Hexylamine was obtained from Aldrich. Hydrobromic acid (48% w/w aqueous) was obtained from Alfa Aesar. Trifluoroacetic acid was obtained from EMD Millipore. Deuterated solvents for NMR (DMSO-d_6 and TFA-d) were purchased from Cambridge Isotopes.

Simulated gastric fluid (SGF) was prepared according to USP 30:[46] 2.0 g of NaCl was dissolved in 7.0 mL of concentrated HCl and 800 mL of deionized water, the pH of the solution was adjusted to 1.2 using 0.1 M NaOH and 0.1 M HCl, and the solution was quantitatively transferred to a 1000 mL volumetric flask and diluted to the mark with deionized water. Simulated intestinal fluid (SIF) was prepared according to USP 26:[47] 6.8 g of KH_2PO_4 and 0.896 g of NaOH were dissolved in 800 mL of deionized water, the pH of the solution was adjusted to 6.8 using 0.1 M NaOH or 0.1 M H_3PO_4, and the solution was quantitatively transferred to a 1000 mL volumetric flask and diluted to the mark with deionized water. An Accumet Basic AB15 pH meter (Fisher Scientific, Waltham, MA) was used for all pH adjustments. Phosphate buffered saline (pH 7.4) was purchased from Fisher Bioreagents as a 10× solution and diluted to 1× using deionized water.

Activated charcoal (−100 mesh particle size, powder) was obtained from Sigma-Aldrich. Acid yellow 3 (a mixture of the mono-, di- and trisulfonic acids of Quinoline Yellow; CAS 8004-92-0) and amitriptyline were purchased from TCI. Acid yellow 3 (AY3) and amitriptyline (ATL) were used as model adsorbates – their chemical structures are given in Fig. S1.†

All cell culture reagents were acquired from ThermoFisher Scientific. RAW 264.7 murine macrophages were cultured in Dulbecco's Modified Eagle Medium with 4500 mg L^{-1} D-glucose, 584 mg L^{-1} L-glutamine, and 100 mg L^{-1} sodium pyruvate (catalog #11995065). This basal media was supplemented with 10% v/v fetal bovine serum (catalog

#26140079) and penicillin streptomycin antibiotics (catalog #15140122) that was diluted to a final concentration of 100 U mL^{-1}. The cells were cultured in an incubator at 37 °C with a humidified atmosphere at 5% CO_2.

2.2 Synthetic procedures

NCA synthesis. α-Amino acid *N*-carboxyanhydride (NCA) monomers were synthesized according to standard literature precedent. Detailed experimental conditions used for preparation may be found in the ESI.†

NCA polymerization. KEY polypeptides were prepared *via* ring-opening polymerization of NCA monomers according to procedures found in literature.[48] A random copolymerization of Lys(Z)-NCA and Glu(OBzl)-NCA was first used to prepare the p[K(*Z*)-ran-E(OBzl)] macroinitiator. The macroinitiator was added to different mole percentages of Tyr(OBzl)-NCA to yield p[(K(*Z*)-ran-E(OBzl))-*b*-Y(OBzl)] with different degrees of aromatic functionalization (*i.e.* KEY10, KEY20, and KEY30). Detailed experimental conditions used for the preparation of the KE macroinitiator and KEY polypeptides may be found in the ESI.†

Polypeptide deprotection. Polypeptides were deprotected following standard literature techniques.[49,50] In a typical deprotection, the protected polypeptide was dissolved in TFA and glacial acetic acid. Then, HBr (48% in water) was added to the flask, resulting in the appearance of a thick white precipitate that redissolved over time. The reaction mixture was stirred at room temperature overnight. The strongly acidic deprotection mixture was safely evaporated to a concentrate using a Schlenk line cold trap and precipitated into tetrahydrofuran (8× the volume of the concentrated copolypeptide solution) while vigorously stirring on ice. The copolypeptide, a white solid, was collected *via* centrifugation, dispersed in deionized water, and dialyzed against deionized water for 4 days using SnakeSkin™ dialysis tubing with a 3500 molecular weight cutoff. Following dialysis, the deprotected copolypeptide was lyophilized to dryness to give a fluffy, white powder and stored at room temperature.

2.3 Characterization techniques

Fourier transform infrared spectroscopy (FTIR). FTIR attenuated total reflectance spectroscopy was performed using a PerkinElmer Frontier FTIR spectrometer with a germanium crystal. Spectra were acquired with a 1 cm^{-1} resolution over a range of 700–4000 cm^{-1}. Using the Spectrum software (PerkinElmer), spectra were corrected for attenuated total reflectance mode, baseline corrected, converted to absorbance, and normalized to the maxima of the amide I peak (1637 cm^{-1} for deprotected KEYs and 1652 cm^{-1} for the protected KEY).

Nuclear magnetic resonance (NMR). A 500 MHz NMR (Bruker Avance™ 500) was used to acquire ^{1}H-NMR spectra of the monomers and polypeptides in DMSO-d^6 and TFA-d, respectively. Data was analyzed using Mestrenova software (version 12.0.1) and TopSpin software (version 4.1.4).

Gel permeation chromatography (GPC). Polypeptide solutions (approximately 10 mg mL^{-1} in dimethylformamide, filtered through a 0.2 μm PTFE membrane) were analyzed *via* gel permeation chromatography with neat dimethylformamide at 25 °C as eluent with a constant flow rate of 1.00 mL min^{-1}. A differential refractive index (RI) detector (Waters and Wyatt) was used, and chromatograms were calibrated to poly(methyl methacrylate) standards.

Zeta potential. Dispersions of the KEYs and activated charcoal were prepared with a concentration of 50 μg mL^{-1} in SGF, SIF, PBS, and deionized water. The dispersions were then loaded into Malvern disposable folded capillary cells (DTS1070). Zeta potentials were measured using a Zetasizer Nano ZS (Malvern Instruments Ltd, Worcestershire, UK) with Zetasizer Software v7.12 (Malvern, Inc.). Three measurements were acquired using the optimal scanning parameters of the instrument (ranging from 10–100 scans per measurement).

Microscopy. Dispersions of each adsorbent (activated charcoal and the KEYs) were prepared with a concentration of 0.1 mg mL^{-1} in SGF, SIF, or PBS. Subsequently, 100 μL of the adsorbent dispersion was dispensed into a well of a 96-well plate. Microscope images of the settled adsorbent particles were acquired on an EVOS® FL Auto Cell Imaging System (ThermoFisher Scientific) with a 10×, 0.30 numerical aperture objective in transmission mode.

Plate reader. A Spark Multimodal Microplate Reader (TECAN) was used to determine the concentration of acid yellow 3 and amitriptyline. Here, 100 μL of the analyte solution was dispensed in a well of a disposable 96-well plate (Greiner Bio-one Cellstar® Cell Culture Plate for acid yellow 3 and Greiner Bio-one UV-Star Microplate for amitriptyline) and analyzed according to the following parameters. For acid yellow 3, absorbance spectra were acquired from 300–600 nm with a step size of 2 nm and a settle time of 50 ms. The λ_{max} for acid yellow 3 was determined to be 412 nm. For amitriptyline, absorbance spectra were acquired from 200–600 nm with a step size of 2 nm and a settle time of 50 ms. The λ_{max} for amitriptyline was determined to be 238 nm.

2.4 Adsorption studies

Adsorption kinetics. In a typical adsorption kinetics experiment, 6 identical adsorbate/adsorbent mixtures were prepared in 1.5 mL Eppendorf tubes as described above using a 5 : 1 ratio of adsorbent-to-adsorbate. The Eppendorf tubes were vortexed briefly to mix and incubated at 37 °C with rotational shaking. At 6 different time points, an Eppendorf was removed from the incubator, centrifuged, and the supernatant was analyzed. The adsorption equilibrium time was designated as the time at which the percent of adsorbate adsorbed became constant. More detail on the experimental conditions used for these studies may be found in the ESI.†

Adsorption capacity. In a typical adsorption capacity experiment, 6 adsorbate solutions were prepared in 1.5 mL Eppendorf tubes, each with a final volume of 250 μL and a concentration ranging from 20–250 μg mL^{-1} (within the linear range of quantification). Next, a dispersion of adsorbent in buffer was added to each Eppendorf to give adsorbent-to-adsorbate ratios ranging from 0.5 : 1 to 22 : 1 and a final

volume of 450 μL. The Eppendorf tubes were vortexed briefly to mix and incubated at 37 °C with rotational shaking. After incubating for the equilibration time (determined from adsorption kinetics experiment), the Eppendorf tubes were removed from the incubator, centrifuged, and the supernatant was plated and analyzed. More detail on the experimental conditions used for these studies may be found in the ESI.†

2.5 Cell culture procedures

Material preparation. Lyophilized powders of KEYs materials as activated charcoal (DARCO, ~100 mesh particle size, Millipore Sigma, catalog #242276) were sterilized in microcentrifuge tubes *via* exposure to 254 nm ultraviolet light for 10 min. Approximately 2–3 mg of all materials was dissolved/dispersed in 1 mL of cell culture media *via* vortexing and sonication. They were then vortexed and diluted to 250 μg mL^{-1} stock solutions.

Cellular vitality experiment. RAW 264.7 macrophages were seeded in the interior wells of 96-well plates at a density of 2×10^4 cells per cm^2. After 2 hours, the cells were considered well-adhered. The media was aspirated and replaced with appropriate volumes of new media and stock solutions to achieve final volumes of 200 μL and the desired concentrations of 250, 100, and 10 μg mL^{-1} for all materials, in triplicate. Cells were allowed to grow in the incubator for 48 hours, and then the vitality assays were performed. Cellular enumeration, vitality, and late necrosis and apoptosis was visualized using fluorescent reporters. The media and materials were aspirated from the wells, followed by two washes with 100 μL of PBS (catalog #10010023, ThermoFisher Scientific). Then the following fluorescent staining solution was added: PBS with 20 mM of Hoechst 33342 (catalog #62249, ThermoFisher Scientific), 2.5 mM of Calcein AM (catalog #C3099, ThermoFisher Scientific), and 1.5 mM of propidium iodide (catalog #J66584-AB, Alfa Aesar). After 10 minutes in the incubator, the staining solution was aspirated and replaced with PBS.

Hoechst 33342 labels the DNA of all cell nuclei and then becomes brightly fluorescent, reporting the number of cells. Upon cellular internalization of Calcein AM, it is converted to a fluorescent form by esterases, reporting vitality. Propidium iodide becomes brightly fluorescent upon binding DNA but is excluded from the nuclei of live cells with intact membranes; thus, it reports dying cells that have not yet detached from the substrate. To quantify the fluorescence of these molecules, we used a fluorescence microplate reader with excitations/emissions of 350/450 nm for Hoechst, 485/525 nm for Calcein AM, and 530/620 nm for propidium iodide. Since this quantification can be unreliable especially with insoluble or fluorescence-altering materials, direct fluorescence imaging using an EVOS® FL Auto Cell Imaging System with a 20×, 0.30 numerical aperture objective was employed. The DAPI channel (visualizes Hoechst) images were used to obtain cell counts with an in-house MATLAB cell counting program, and these counts were used to quantify percent vitality.

3. Results and discussion

3.1 Polypeptide-based adsorbent design considerations

KEY polypeptide adsorbents were prepared with K (lysine), E (glutamic acid), and Y (tyrosine) amino acid residues. This amino acid composition was selected to create functional adsorbent polypeptides that are (1) adhesive to drug molecules, (2) cohesive to form discrete adsorbent particles, and (3) cytocompatible (Fig. 1).

In the context of macromolecular adsorbents, adhesion is defined as the affinity of an absorbate to the surface of the adsorbent particle. The clinical standard, AC, was used as a

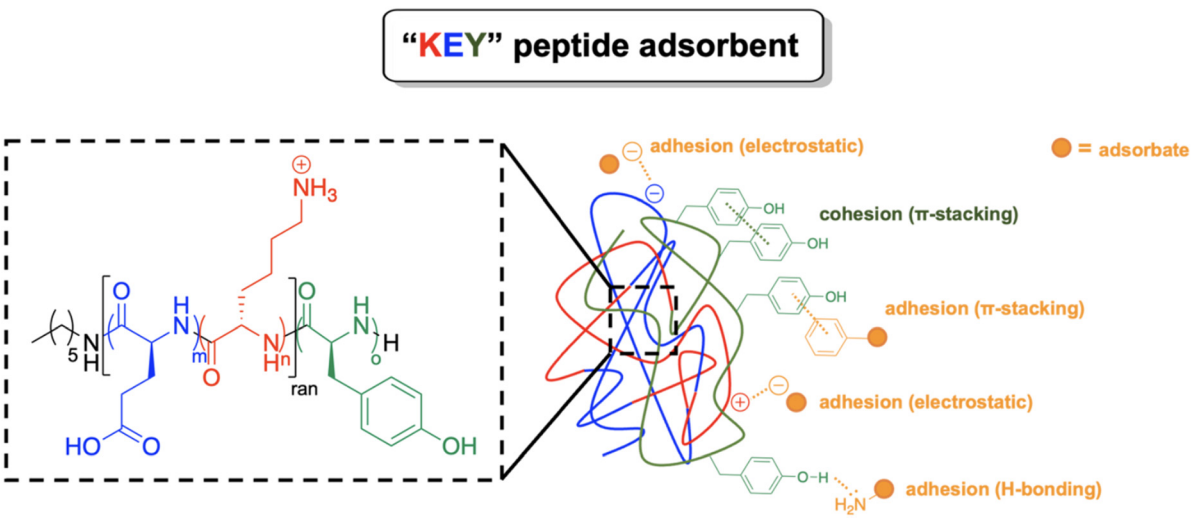

Fig. 1 KEY aromatic polypeptide amphiphiles are designed to impart adhesion, cohesion, and cytocompatibility to the macromolecular drug adsorbent.

model to achieve adhesion in a polypeptide-based adsorbent. AC has a honeycomb lattice framework which primarily adsorbs molecules through π–π interactions with the aromatic drug molecule.[6] Hydrogen bonding and electrostatic interactions can also occur between AC and the drug molecule, which further encourages adsorption.[6] To emulate the adsorption mechanism of AC, polytyrosine (Y) was used as the hydrophobic block in the KEYs as a strategy to promote adsorption of aromatic drugs to the aromatic tyrosine residues through π-stacking. In addition, the polypeptide backbone can participate in hydrogen bond interactions. The pendant groups on the amide backbone also afford dynamic hydrogen bond capabilities in a pH-dependent manner. Further, the pH of the solution can influence electrostatic adsorption of drug molecules to the polypeptide. Since KEYs contain positively and negatively charged residues, electrostatic attraction may be harnessed to target drugs in certain pH conditions based on pK_a.

Cohesion—defined as the affinity of a molecule to itself—allows a macromolecular adsorbent to form an aggregate that engulfs and sequesters the adsorbed drug. KEYs are designed to possess cohesion due to the identity and balance between their hydrophobic and hydrophilic blocks. The Y block of the polymer promotes cohesion through π-stacking interactions between hydrophobic tyrosine residues. However, extensive cohesion is unfavorable as it decreases dispersibility which limits the available surface area for adsorption. To balance cohesion with dispersibility, the KEYs possess a poly(lysine-*co*-glutamic acid) (KE) block, which mediates the cohesion of the Y block due to its pH-responsive affinity for aqueous solvent. Thus, tuning the stoichiometry of the hydrophobic and hydrophilic blocks in the KEYs offers control over the balance between cohesion and dispersibility of the KEY aggregates.

Several amino acids are capable of adhesive π-stacking interactions such as phenylalanine, tryptophan, histidine, and tyrosine. However, tyrosine was selected for inclusion in KEYs based on its physical and chemical properties compared to other eligible residues. KEYs are designed as amphiphiles; this precluded the use of histidine in the hydrophobic block since it is relatively hydrophilic. Phenylalanine is reported to have extensive cohesion and is less hydrophobic than tyrosine.[51,52] Alternatively, tryptophan is more hydrophobic than tyrosine, but has few cohesive interactions.[51,52] Therefore, tyrosine was selected for use in the hydrophobic block since it is hydrophobic and features a moderate level of cohesion. The hydroxyl group of tyrosine is also capable of functioning as a hydrogen bond donor and acceptor, further positioning the residue for use in the adsorption drugs.

Cytocompatibility is crucial for macromolecular drug adsorbents intended for human consumption. Polypeptides were chosen as the basis for KEYs since they are essential biological motifs which can be derived from natural sources. However, some studies suggest that synthetic polypeptides may elicit toxicity depending on pendant group stereochemistry.[53–55] Synthetic polypeptides have also been reported to provoke immune responses through nonspecific binding with molecules such as opsonins.[56] The polypeptides were designed with these considerations in mind. KEYs are prepared using biologically occurring (L)-enantiomeric amino acids, as (D)-enantiomeric residues have been speculated to demonstrate toxicity. The KE block of the polymer also features zwitterionic pendant groups of which studies have shown to prevent non-specific binding with native biomolecules, thereby negating toxicity.[57–62]

3.2 Structural characterization of KEYs

The KEYs were synthesized using a ring-opening polymerization (ROP) of α-amino acid *N*-carboxyanhydride (NCA) monomers.[63] First, a copolymerization between Lys(*Z*)-NCA and Glu(OBzl)-NCA was performed to prepare the hydrophilic block of the KEY polypeptide. Previous literature indicates that Glu(OBzl)-NCA reacts 3.6 times faster than Lys(*Z*)-NCA during the copolymerization of γ-benzylglutamate (E; $r_1 = 1.87 \pm 0.31$) and ε-carbobenzoxylysine (K; $r_2 = 0.52 \pm 0.11$).[48,56] The resulting copolymer deviates slightly from ideal copolymerization kinetics (as suggested by the product of r_1 and r_2) and contains a larger mol percentage of Glu(OBzl) in all cases at low conversion. However, at approximately 30% conversion, the higher concentration of Lys(*Z*)-NCA balances the reactivity of Glu(OBzl)-NCA to yield a relatively constant copolymer composition from the initial monomer feed ratio. The KE macroinitiator was then added to different monomer feed ratios of Tyr(OBzl)-NCA to yield three KEY formulations (KEY10, KEY20, and KEY30).

Each of the protected KEY formulations demonstrated bimodal traces when analyzed by GPC (Fig. S5†). The peaks at low elution volume greatly overestimate the expected molecular weights of the polypeptides. These signals are attributed to aggregates formed by the self-assembly of polypeptides in solution. This behavior commonly occurs with biopolymers during GPC and is detailed in literature.[64,65] Many reports correlate aggregation to hydrophobic associations[66,67] and intermolecular hydrogen bonding.[68,69] Thus, it is reasonable for KEYs to aggregate during GPC measurements, considering their chemical compositions. Huesmann *et al.* studied this phenomenon using polypeptides, demonstrating that aggregation in GPC occurs as chain length increases due to shifts in secondary structure.[70] This would explain why the major peak of KEY10 appears at high elution volume, but the major peaks of KEY20 and KEY30 appear at low elution volume. KEY10 exhibits a lower tendency for aggregation since the chain length of tyrosine is shorter compared to KEY20 and KEY30. This model indicates that there is a critical length at which a secondary structure transition occurs, driving in aggregation.[71] Based on dispersity, there would always be a peak at the same high elution volume which represents the part of the molecular weight distribution that is below the secondary structure transition. This would explain why the minor peaks from KEY20 and KEY30 roughly align with the major peak of KEY10.

The dispersity of the major and minor peak for each polypeptide is listed in Table 1 as either $Đ_{low}$ or $Đ_{high}$, where the

Table 1 Structural characterization of KEY polypeptides

ID	Synthetic target	$Đ_{low}$ [a]	$Đ_{high}$ [a]	DP K [b]	DP E [b]	DP Y [b]	Target M_n [c] (kDa)	Actual M_n [c] (kDa)	Mol % Y
KE initiator	$p(K_{20}\text{-}E_{20})$		1.16	20	20		5.25	5.47	
KEY10	$p(K_{20}\text{-}E_{20}\text{-}Y_{10})$	1.15	1.16	20	20	8	6.88	6.81	16
KEY20	$p(K_{20}\text{-}E_{20}\text{-}Y_{20})$	1.38	1.09	20	20	20	8.51	8.77	32
KEY30	$p(K_{20}\text{-}E_{20}\text{-}Y_{30})$	1.66	1.09	20	20	29	10.14	10.24	41

[a] Dispersity ($Đ$) determined from GPC. [b] Degree of polymerization (DP) determined from ^{1}H NMR end group analysis. [c] M_n determined from ^{1}H NMR end group analysis.

subscript indicates the relative elution volume at which the signal appears. It is unlikely that the values provide accurate representations of polymer dispersity considering that none of the peaks represent the entire molecular weight distribution of the sample, except for the KE macroinitiator. Differences in the number of aggregated polymer chains also contribute to the broad size distributions of the peaks at low elution volume. However, the aggregate peaks follow the expected trend in molecular weight with elution volume and provided tentative evidence that the KEYs were prepared successfully.

Characterization by quantitative ^{1}H NMR confirmed that the polypeptides possess controlled amino acid composition and expected macroscopic sequences (Table 1). The number of pendant group protons were correlated to the number of backbone protons to determine degree of polymerization and to confirm the success of each reaction. In the spectra acquired before and after deprotection, the number of protons align with theoretical expectations based on structure (Fig. S6 and S7†). Characterization by ^{1}H NMR indicates that KEYs are pure, which strongly supports the argument of peptide aggregation during GPC. ^{1}H NMR was also employed to quantify the degree of deprotection for each polypeptide. Following deprotection, the number of aromatic protons were compared with theoretical expectations to determine the percent conversion from protected peptide. FTIR spectra were acquired to supplement ^{1}H NMR data and confirm the successful deprotection of each polypeptide (Fig. S8†). The spectra of deprotected compounds contained O–H stretching (3500 cm^{-1}) from glutamic acid and O–H bending (1400 cm^{-1}) from tyrosine. Deprotected compounds were also characterized by the lack of a carbamate signal from the lysine protecting group (1750 cm^{-1}). Together, this data validated the successful preparation of KEY polypeptides.

Many studies demonstrate that electrostatic interactions dictate adsorption in systems involving charged particles.[30] KEYs were designed with amino acid residues of opposite charge (KE) and are expected to exhibit a pH-responsive dynamic surface charge in biological conditions. This was confirmed by measuring the zeta potential of each formulation in simulated biological environments (Fig. 2). Data obtained from dynamic light scattering (DLS) experiments are consistent with theoretical expectations based on pK_a. In simulated gastric fluid (SGF; pH 1.2), the KEYs exhibit a positive charge because the pH is below the pK_a of all residues. In contrast, the KEYs are negatively charged in simulated intestinal fluid (SIF; pH 6.8) and phosphate-buffered saline (PBS; pH 7.4)

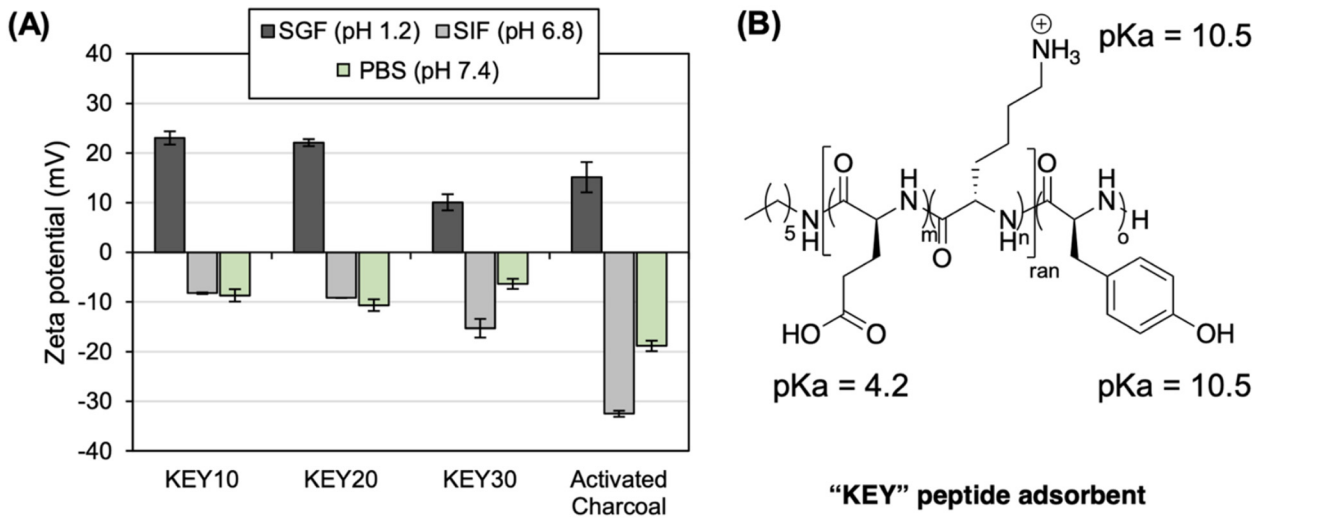

Fig. 2 The zeta potential of the KEY aggregates is dictated by pH. (A) Zeta potential of adsorbates (KEYs and AC) in simulated gastric fluid (SGF), simulated intestinal fluid (SIF), and phosphate buffered saline (PBS). (B) The pK_a of each amino acid residue in the KEY dictates the overall surface charge of the KEY aggregates in different media.

because the pH is above the pK_a of glutamic acid. Dynamic surface charge is also observed for activated charcoal, as it features a variety of acidic functional groups.

Electrophoretic mobility was converted to zeta potential using the Smoluchowski approximation which is typically employed for measurements in aqueous media.[72] This limit is contingent upon the particle size being much larger than the Debye length.[73] However, the approximations of the Smoluchowski limit are inaccurate at high salt concentration, meaning that the zeta potential values obtained in SGF, SIF, and PBS may not appropriately characterize the properties of the KEYs.[74] Thus, measurements were also performed in deionized water to provide more information regarding the electrokinetic potentials of the polypeptides (Fig. S14†). Since the pH of deionized water is above the pK_a of glutamic acid, the zeta potentials of the KEYs are all negative. The zeta potentials for the KEYs in deionized water are more negative than in electrolyte solutions because salts form a screening cloud around particles in solution. This reduces the effective zeta potential as the particle is shielded from electrostatic force by counter ions. These results are in line with theoretical expectations based on literature[75] and offer a more comprehensive understanding regarding the physical properties of KEYs.

When the KEYs are added to aqueous media, they spontaneously form amorphous aggregates that can be dispersed by manual shaking (Fig. 3). This solution preparation method is realistic in clinical conditions, where controlled nanoparticle formation by gradual solvent swap would be impractical. In theory, the amorphous assemblies of KEYs may be advantageous for the target application. Amorphous materials typically have weak attractive forces between polymer chains. This prevents excessive cohesion between molecules in solution and increases the surface area for drug adsorption.[76] The weak forces between chains also limit the packing densities of these materials which could discourage material deposition in solution.[77] Due to their disordered structures, amorphous materials also contain internal free volume. This makes them more susceptible to solvent penetration which is beneficial for the adsorption of drugs which are dissolved in solution.[76,78]

Overall, higher hydrophobic content (*i.e.*, KEY30) imparts cohesion that is manifested in the formation of larger KEY aggregates, while lower hydrophobic content (*i.e.*, KEY10) results in KEY aggregates with greater dispersibility. KEY30 is the least dispersible in aqueous media. It forms irregularly shaped aggregates up to 280 mm in length – regardless of pH – due to its larger mole fraction of Y that drives cohesion. KEY10 and KEY20 have lower mole fractions of Y and exhibit higher dispersibilities in SIF and PBS, forming aggregates that are less than 150 mm in length. Importantly, KEY20 forms smaller particles ranging from 15 to 125 mm in SGF while KEY10 is fully soluble in SGF.

A control experiment was performed to validate the impact of the Y block in the formation of KEY aggregates. Here, polyKE poly[$(lysine)_{20}$-*co*-$(glutamic\ acid)_{20}$] (with no hydrophobic Y block) was dispersed in SGF, SIF, and PBS. In all three media, polyKE was completely soluble, resulting in a

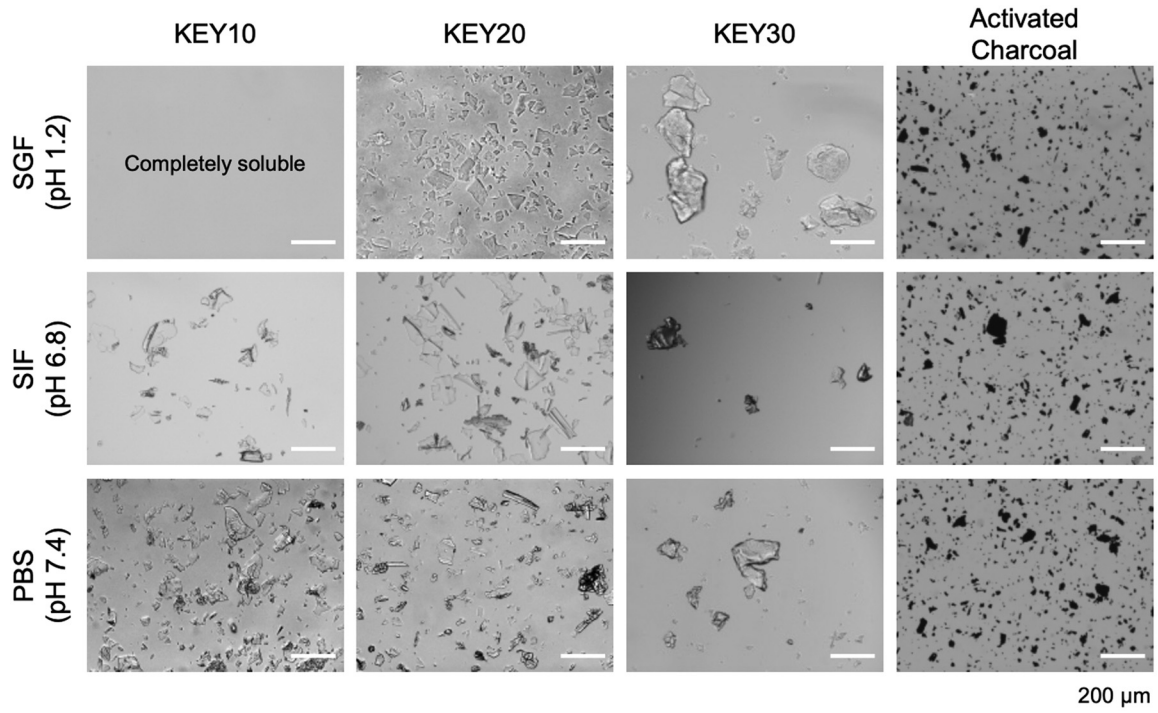

Fig. 3 Microscopy of KEY polypeptides compared to activated charcoal in different simulated biological media. KEYs aggregates are amorphous and do not appear as ordered assemblies.

clear and colorless solution, suggesting that aggregation of the KEYs in these media is driven by the polytyrosine block (Fig. S9†). This result is expected because the ionic strength of the simulated body fluids – SGF (106 mM), SIF (322 mM), and PBS (200 mM) – is significantly higher than the ionic strength of the KEY dispersion (14–31 mM, depending on the formulation). As a result, polyion complexation between the cationic lysine residues and anionic glutamic acid residues is largely screened by the high concentration of ions in the media.

After characterization, KEYs were studied to understand how the structure–function relationships of the polypeptides translate in the context of drug adsorption from simulated digestive media. The method of quantifying adsorption relies on insoluble adsorbent particles that can be removed from the system after adsorbing the drug. As such, the adsorption performance of KEY10 could not be assessed in SGF due to its solubility in this media.

3.3 Adsorption kinetics

Adsorption studies were performed to assess the rate at which the KEYs and AC adsorbed acid yellow 3 (AY3) and amitriptyline (ATL). The structures for both model compounds can be found in Fig. S1.† Kinetics experiments were conducted using a constant ratio of 5 : 1 (w/w) of adsorbent-to-adsorbate in either SGF, SIF, or PBS. For each experiment, replicate samples of each adsorbent/adsorbate mixture were incubated at 37 °C with rotational stirring. At various time points, a sample was centrifuged to pellet the insoluble adsorbent particles and the amount of adsorbed compound was quantified by measuring the concentration of free adsorbate in the supernatant *via* UV-Vis spectroscopy (Fig. S10†). For all adsorbent, adsorbate, and media combinations, adsorption equilibrium is reached in 5 to 20 minutes (Fig. 4).

In clinical settings, the majority of adsorption ideally occurs prior to gastric emptying; before the stomach contents

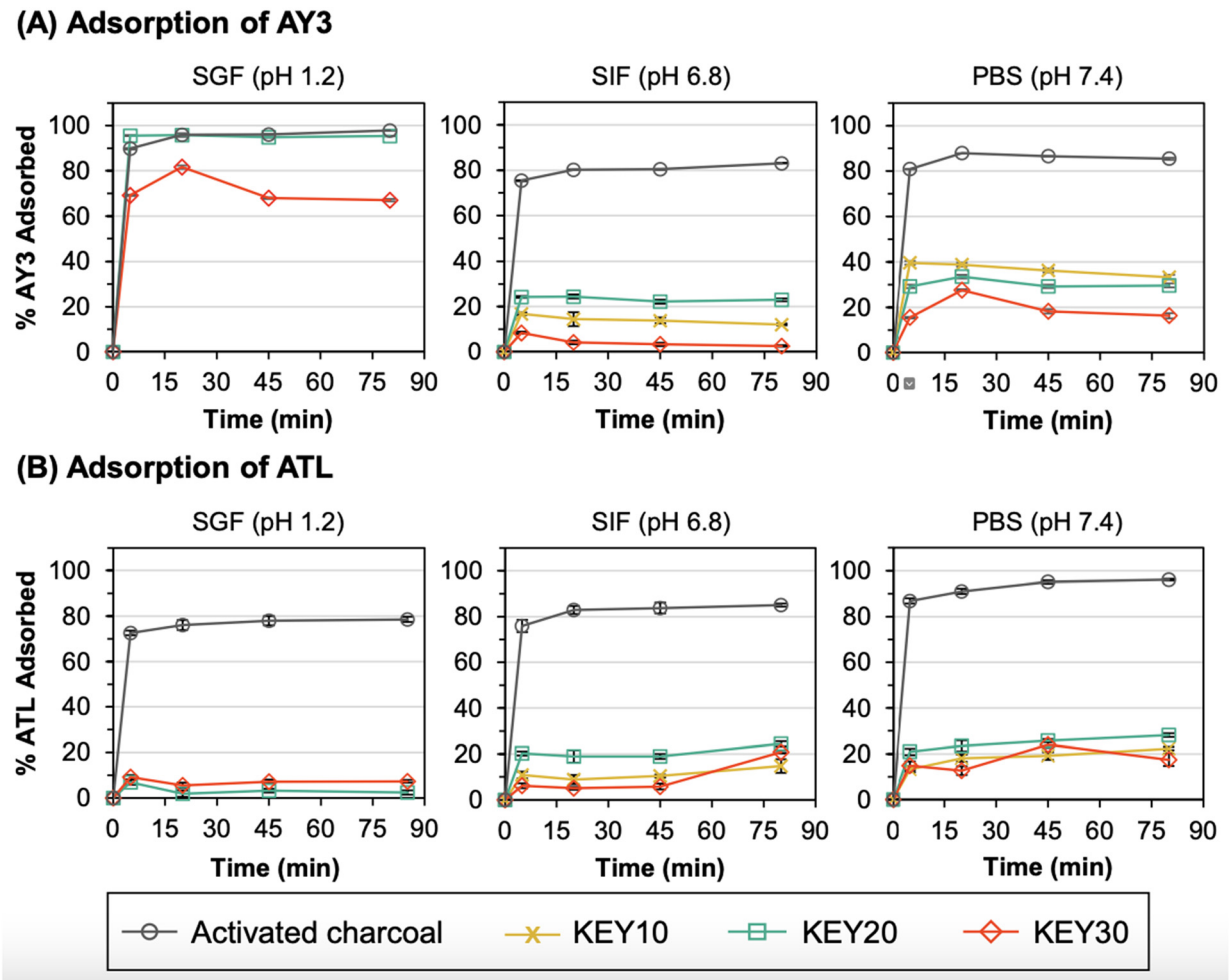

Fig. 4 Adsorption kinetics of (A) acid yellow 3 (AY3) and (B) amitriptyline (ATL) to the KEYs and AC. Samples were prepared in simulated gastric fluid (SGF, pH 1.2), simulated intestinal fluid (SIF, pH 6.8), and phosphate buffered saline (PBS, pH 7.4) with a 5 : 1 ratio of adsorbent-to-adsorbate and incubated at 37 °C. Note that error bars represent the standard deviation of three replicate measurements. All data points have error bars, but some are too small to be visualized. In some cases, the % adsorbed is observed to decrease which may be explained by the reversibility of van der Waals forces.

are transferred to the intestines and absorbed into the blood. Therefore, the performance of KEYs in SGF is of utmost importance, followed by SIF. In SGF, KEY20 and AC exhibited similar adsorption capacities for AY3 (Fig. 4a). The excellent adsorption capability of KEY20 for AY3 is rationalized primarily through electrostatic interactions and π–π stacking. In SGF, KEYs exhibit a positive surface charge because all KEY residues are protonated. Under these conditions, positively charged lysine pendant groups (pK_a = 10.5) exhibit a high affinity towards negatively charged sulphonic acid groups ($pK_a \sim -7$). This explains the lower adsorption observed in SIF and PBS, where there is repulsion between negatively charged sulphonic acid and deprotonated glutamic acid moieties (pK_a = 4.2). To evaluate whether electrostatic interactions are present in adsorption process, control experiments were performed with KEYs and AY3 in SGF under an elevated concentration of NaCl (20 additional mg mL^{-1}). Salt was expected to interrupt the mechanism of adsorption to KEYs through electrostatic interactions with either the adsorbent or adsorbate. After 20 minutes of incubation in SGF, the vials were processed following the standard experimental conditions used in this study. The solution with a higher salt concentration was visibly more yellow, suggesting that less AY3 had been adsorbed (Fig. S11†). This was confirmed using UV-Vis spectroscopy, which demonstrated that the concentration of AY3 was higher in the solution containing more salt (10.6 μg mL^{-1}; 2.1% remaining) *versus* the standard solution of SGF (0.4 μg mL^{-1}; 0.1% remaining).

Electrostatic interactions with KEYs depend on salt concentration, meaning that reliance upon this mechanism of adsorption may be unrealistic *in vivo*, where salt levels vary widely based on diet. This highlights the importance of alternative intermolecular interactions for KEYs to perform as effective drug adsorbents. KEYs were designed based on AC as a model, which features a large, delocalized network which is available for π-stacking interactions. Many studies demonstrate based on the Hunter–Sanders model that stronger π-stacking interactions occur when electron-withdrawing substituents are found on aromatic groups.[79–81] This is due to a decrease in π-electron density of the conjugated network which relieves π–π repulsion. AY3 bears 1–3 sulphonic acid groups in its π-system. In theory, these features strongly withdraw electron density from the conjugated network and further promote adsorption *via* π-stacking to aromatic residues.

AY3 served as a model compound for evaluating the feasibility of chemical adsorption to KEYs. However, KEYs are designed primarily for use with aromatic drugs. After determining the performance of KEYs with AY3, the next logical step was to evaluate their performance with compounds of interest. Amitriptyline (ATL) belongs to a commonly prescribed class of drugs called "tricyclic antidepressants" and was chosen as a representative compound which would be treated using KEYs in clinical settings.[82]

Importantly, KEYs adsorbed ATL during incubation which provides proof of concept that polypeptides are capable of adsorbing antidepressants (Fig. 4b). Although KEYs displayed a lower affinity for ATL compared to AY3 in all media, these results offer important and necessary insights into the mechanism of adsorption to KEYs. As with AY3, the adsorption of ATL by KEYs can be rationalized through electrostatic interactions and π-stacking. ATL (pK_a = 9.8) is electrostatically repelled by lysine in all test conditions but is electrostatically attracted to glutamic acid in SIF and PBS. This accounts for its higher adsorption in these simulated biological media. However, ATL bears no strongly electron-withdrawing substituents in its conjugated π-system which may translate to lower aromatic stacking. Current KEY formulations also possess relatively low mol percent formulations of tyrosine, which likely limit adsorption by π-stacking interactions. Future formulations plan to incorporate higher mole percentages of tyrosine into the polypeptides to encourage this mechanism of adsorption. For compounds which do not have high electrostatic attraction to the polypeptides (such as ATL) this would increase the number of available sites to which adsorbates are able to bind.

The performance of KEYs with AY3 and ATL highlights the chemical characteristics which enhance adsorption to polypeptides. Attractive electrostatic interactions were observed to increase adsorption capacity. Aromatic compounds with electron withdrawing substituents also exhibit higher adsorption to KEYs in agreement with theoretical expectations based on the Hunter–Sanders model. However, adsorption to KEYs is low for aromatic drugs which exhibit repulsive interactions and for compounds which have no electron withdrawing substituents. In these cases, higher adsorption is likely to be achieved through greater aromatic functionalization of the KEY polypeptide adsorbent.

3.4 Adsorption at different adsorbent-to-adsorbate ratios

Next, adsorption of AY3 and ATL to the KEYs and AC was evaluated at different ratios of adsorbent-to-adsorbate. Adsorption to AC is a reversible process that is based on an equilibrium between free drug and the AC–drug complex. As a drug overdose intervention, medical experts typically recommend dosing AC at a 10 : 1 (w/w) ratio of AC-to-toxin to shift the adsorption equilibrium towards the AC–drug complex, thereby limiting desorption.[83] However, the exact dose of toxin that caused the overdose is not always known. As such, it is important to evaluate the adsorption capacity of an adsorbent at a variety of adsorbent-to-adsorbate ratios.

Trends in these adsorption capacity experiments reinforce the trends from the adsorption kinetics experiments and demonstrate the capability of the KEYs to adsorb the model adsorbates at a range of adsorbent-to-adsorbate ratios. For adsorption of AY3 in SGF, KEY20 and KEY30 exhibited similar adsorption capacities to AC (Fig. 5). Again, this result is likely due to a combination of electrostatic attraction and π-stacking between the KEYs and AY3. Overall, this result indicates that the KEY formulation, as it stands, is advantageous over AC for the adsorption of negatively charged, aromatic drugs from acidic gastric fluid.

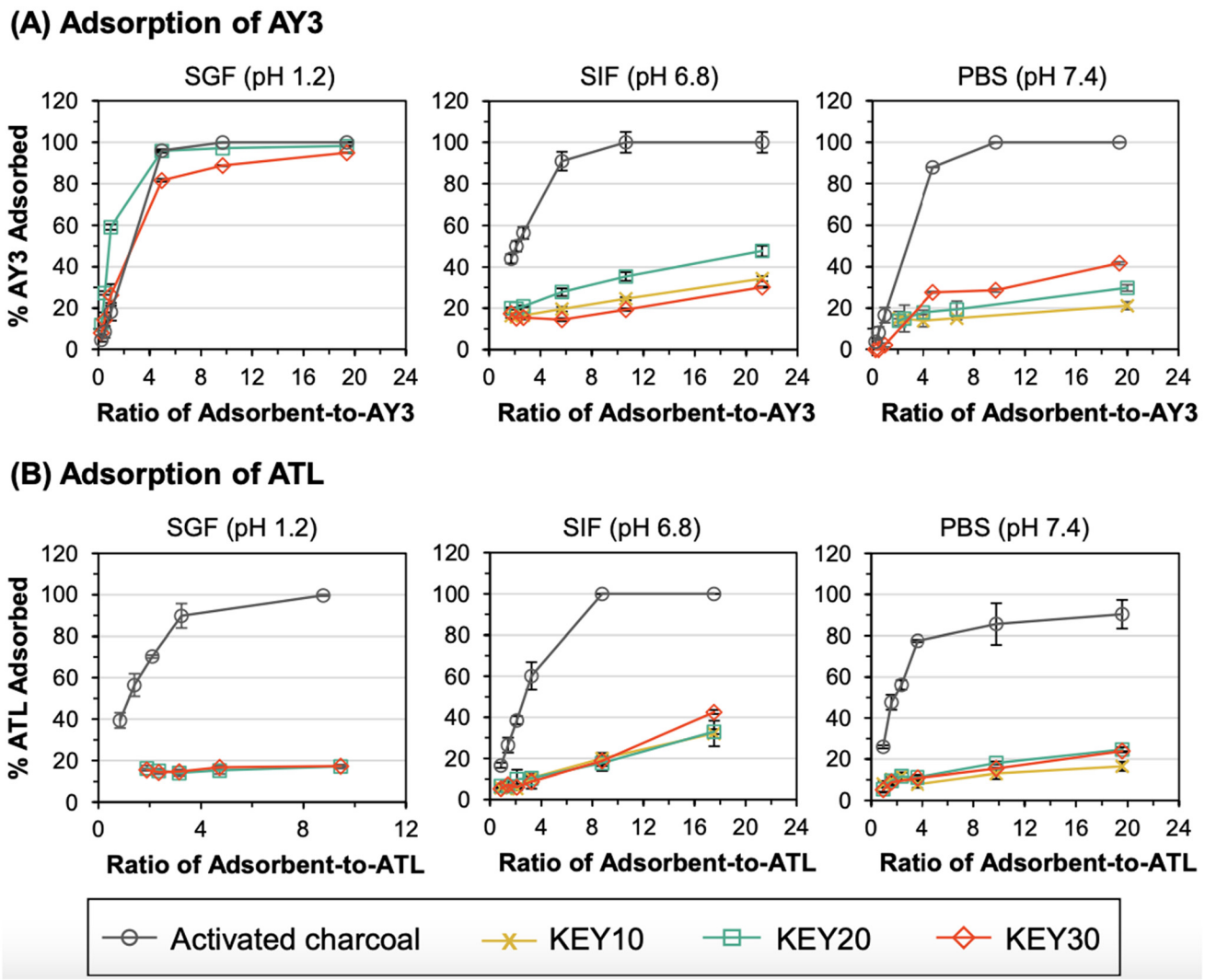

Fig. 5 Adsorption capacity of acid yellow 3 (AY3) (A) and amitriptyline (ATL) (B) by AC and the KEYs are compared at different ratios of adsorbent-to-adsorbate. SGF is simulated gastric fluid (pH 1.2), SIF is simulated intestinal fluid (pH 6.8), and PBS is phosphate buffered saline (pH 7.4). Samples were incubated at 37 °C for 20 minutes before analysis. Note that error bars represent the standard deviation of three replicate measurements. All data points have error bars, but some are too small to be visualized.

Consistent with the results from the adsorption kinetics experiments, KEY20 and KEY30 were less effective at adsorbing ATL from SGF, compared to AC. As discussed, this is thought to be caused by electrostatic repulsion between the cationic KEYs and cationic ATL. The stark difference in adsorption performance of AY3 and ATL in SGF suggests the possibility of further tuning the KEY design to selectively adsorb specific adsorbate targets, where the charge of the adsorbate is considered in the selection of the amino acid composition of the polypeptide-based adsorbent.

In SIF and PBS, the KEYs were less effective at adsorbing AY3 and ATL, compared to AC; and the adsorption capacity of the KEYs was dependent on the molarity of the media, further indicating that electrostatic interactions play a large role in the adsorption mechanism of the KEYs. When ions are present in the media, they form an electrical double layer around the charged adsorbent and adsorbate surfaces, leading to a suppression of electrostatic interactions between the adsorbent and adsorbate.[84] The molarity of SIF (72 mM) is less than half of PBS (150 mM). Generally, the KEYs adsorbed AY3 and ATL more effectively in SIF, compared to PBS. This indicates that electrostatic attraction plays a large role in the adsorption mechanism of the KEYs. The higher concentration of ions in PBS, relative to SIF, results in lower adsorbate–adsorbent binding because ions from the media act as a charge screen to suppress their electrostatic interactions. The one exception to this trend lies in the adsorption of AY3 by KEY30, where the adsorption capacity is higher in PBS relative to SIF. This result suggests that electrostatic interactions play a smaller role in the adsorption mechanism of KEY30, compared to KEY10 and KEY20. This is reasonable given that KEY30 has the lowest molar ratio of hydrophilic block (which is the source of charge) out of all the KEYs. Because of this, π–π stacking is expected to have a greater influence on adsorption than electrostatics for KEY30.

3.5 Adsorption modelling

The maximum adsorption capacity and the relative affinity of the adsorbate–adsorbent pair can be extrapolated by fitting adsorption data to an isotherm model. This analysis provides insight into the adsorption mechanism. The Langmuir isotherm model is one of the most commonly used approaches to model adsorption of a variety of adsorbates to AC.[36,85–89] The Langmuir model offers advantages over other isotherm models (such as the Freundlich or the Redlich–Peterson models) because it can be used to calculate a predicted maximum adsorption capacity of the system.

The Langmuir isotherm model describes monolayer adsorption onto a homogenous adsorbent surface and is described by eqn (1) (non-linear form) and eqn (2) (linear form), where Q_e is the adsorption capacity at equilibrium (mg adsorbed per g of adsorbate), Q_m is the maximum adsorption capacity, C_e is the concentration of free adsorbate at equilibrium, and K_L is the Langmuir constant.[90] For non-linear Langmuir fitting, the goodness of fit was determined by calculating the χ^2 value according to eqn (3), where $Q_{e,exp}$ is the experimental Q_e value and $Q_{e,calc}$ is the Q_e value calculated by the fit.

$$Q_e = \frac{Q_m \times K_L \times C_e}{1 + K_L \times C_e} \quad (1)$$

$$\frac{C_e}{Q_e} = \frac{C_e}{Q_m} + \frac{1}{K_L \times Q_m} \quad (2)$$

$$\chi^2 = \sum \frac{(Q_{e,exp} - Q_{e,calc})^2}{Q_{e,calc}} \quad (3)$$

The experimental adsorption data was fit to both the non-linear form and linear form of the Langmuir isotherm model. In most cases, the experimental adsorption data fit both the non-linear and linear forms of the Langmuir isotherm model fit, producing a low χ^2 values (for non-linear fits) and R^2 values greater than 0.75 (for linear fits) (Table S1†) and allowing calculation of Q_m and K_L values. However, only the Q_m and K_L values from the non-linear Langmuir fitting are reported because: (1) in most cases, these values were in agreement with those obtained by linear fitting; (2) error in the Q_m values obtained by non-linear fitting was consistently lower than error in the Q_m values obtained by linear fitting; and (3) previous researchers have reported that non-linear fitting results in a significantly lower mean of the error function and thus is a better representation of experimental results, compared to linear fitting.[90,91] A summary table comparing the results of non-linear *versus* linear Langmuir fitting is provided in Table S2, and the non-linear Langmuir fits are given in Fig. S12–13.† In one instance (AY3 adsorption by AC in SIF), the Q_m values obtained by the non-linear and linear Langmuir fits agreed; but the K_L value produced by the non-linear fit approached infinity, which is erroneous. As such, the Q_m and K_L values calculated from the linearized Langmuir isotherm were reported for this condition.

For three of the adsorption data sets – KEY30/AY3/PBS, KEY30/AY3/SIF, KEY20/ATL/SGF – neither the non-linear nor the linearized versions of the Langmuir isotherm model produced a satisfactory fit. This result indicates that adsorption in these conditions is non-Langmuirian, which could be caused by the poor dispersibility of KEY30 in PBS and SIF and electrostatic repulsion between cationic KEY20 and cationic ATL in SGF. As such, the values derived from these poorly fitted isotherms were excluded from the discussion below.

The maximum adsorption capacities (Q_m) of the adsorbate–adsorbent pairs support the trends observed in the previous two sections (Fig. 6). Generally, AC had a higher adsorption

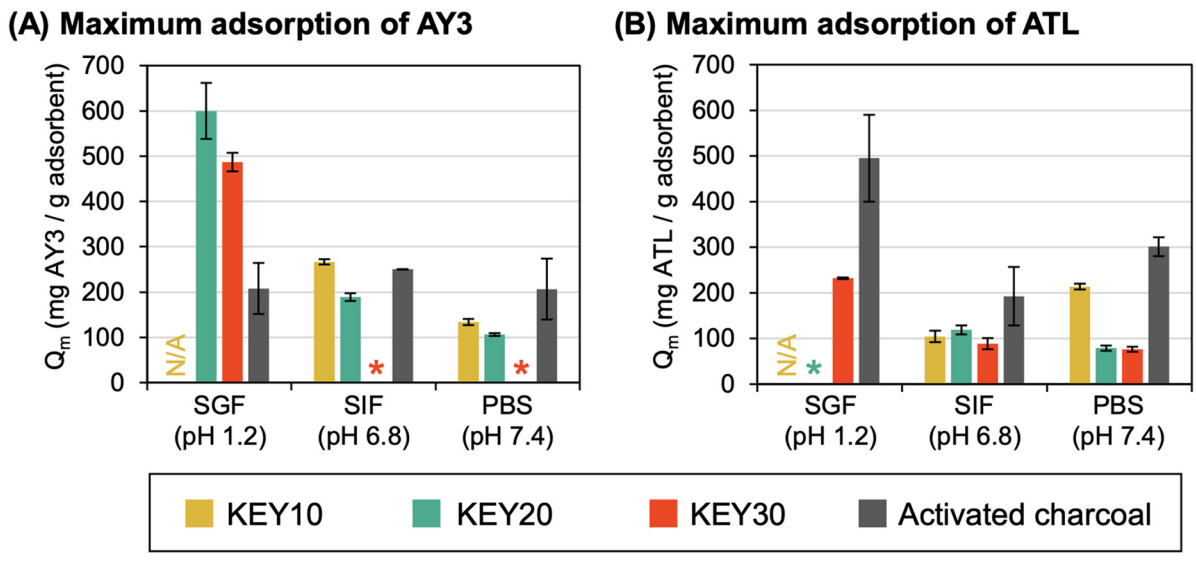

Fig. 6 Maximum adsorption capacity (Q_m) of (A) acid yellow 3 (AY3) and (B) amitriptyline (ATL) by the KEYs and AC at different pH as determined by Langmuir isotherm fitting. SGF is simulated gastric fluid (pH 1.2), SIF is simulated intestinal fluid (pH 6.8), and PBS is phosphate buffered saline (pH 7.4). Asterisks (*) indicate conditions that could not be determined due to poor fitting to the Langmuir isotherm model.

capacity of AY3 and ATL in a neutral pH (SIF and PBS), compared to the KEYs; however, the difference in their adsorption capacity was not tremendous. For example, the adsorption capacity of KEY20 was 119.0 mg ATL per g in SIF, while AC adsorbed up to 192.9 mg ATL per g. The KEYs exhibited adsorption capacities within one order of magnitude of AC in all conditions tested. Remarkably, KEY20 and KEY30 outperform AC in the adsorption of AY3 in SGF: the maximal adsorption capacities of KEY20 and KEY30 were 599.9 mg AY3 per g and 487.2 mg AY3 per g, respectively, while AC only adsorbed 208.1 mg AY3 per g. This result demonstrates the promise of polypeptide amphiphile-based drug adsorbents and suggests that rationally designed adsorbent–adsorbate pairs can achieve excellent adsorption capacities.

The Langmuir constant, K_L, was used to establish that the adsorption capacity of the KEYs is limited by their low surface area. K_L is related to the affinity between an adsorbent–adsorbate pair, and a higher K_L value is indicative of a more favorable adsorption process.[6] K_L can be correlated with the variation of surface area and porosity of the adsorbents, implying that a larger surface area and pore volume result in a higher affinity between the adsorbent and adsorbate.[91] Previous studies have shown that the surface area of self-assembled, nano-porous polypeptide structures to be between 41.7–56.8 $m^2\ g^{-1}$.[92] AC, on the other hand, has exceptionally high surface area (950–2000 $m^2\ g^{-1}$), which is a major contributing factor to its high adsorption capacity.[93] We determined that AC had K_L values that were 1–3 orders of magnitude higher than the KEYs in all conditions tested (Fig. 7). Because AC has a significantly higher surface area than the KEYs, it is reasonable that AC has a high affinity for the adsorbates (K_L value) regardless of the adsorbate and the media. This result further underscores that the KEYs' adsorption performance is limited by their low surface area and suggests that the design of future generations of KEYs should target three-dimensional polypeptide aggregates with higher surface area.

3.6 Cytocompatibility

As a preliminary safety assessment, we evaluated the *in vitro* cytocompatibility of the KEY adsorbents and AC using RAW 264.7 murine macrophages. This cell type was selected as a model because of its involvement in the body's initial immune response towards foreign materials. While exposure to drug adsorbents would primarily be limited to the gastrointestinal tract lining, it is possible for the KEYs to be metabolized and absorbed into the bloodstream. Therefore, it is important to probe the cytocompatibility of these materials with mammalian cells.

The vitality of the macrophages was assessed both quantitatively and qualitatively after two days of exposure to dispersions of KEY10, KEY20, KEY30, or AC in cell media at concentrations of 10, 100, and 250 μg mL^{-1}. As a quantitative measure, cellular vitality was determined by counting the number of living cells with an in-house MATLAB image analysis program present after two days of growth in each culture condition. This metric combines the effects of both cell proliferation and viability. Fluorescence microscopy was used to qualitatively assess the health of the cells. Here, Hoechst (blue) was used to stain the nuclei of living cells, Calcein AM (green) was used to visualize the cytoplasm of cells engaging in healthy metabolic activity, and propidium iodide (red) was used to stain cells that are dying.

Exposure to the KEYs at all tested concentrations was found to yield no statistically significant reduction in cellular vitality, indicating good *in vitro* cytocompatibility (Fig. 8A). Activated charcoal, on the other hand, was found to significantly reduce cellular vitality at 100 and 250 μg mL^{-1}. This reduction of cellular vitality upon exposure to AC is an expected result because activated charcoal is known to have poor side effects *in vivo*,[83,94,95] which is often accompanied by cytotoxicity to one or multiple types of cells. Fluorescence microscopy images (Fig. 8B) show good cell health following exposure to the KEYs

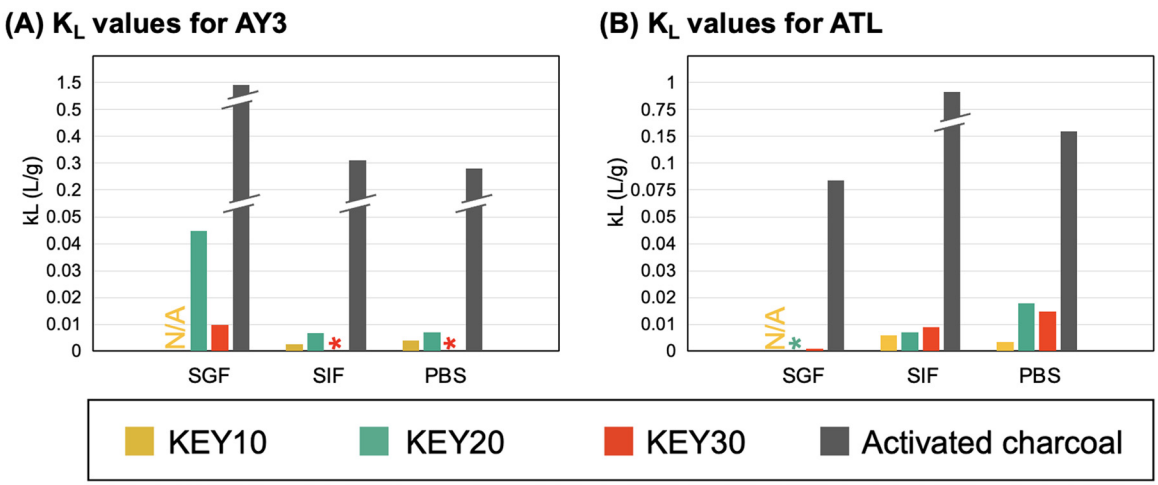

Fig. 7 K_L values calculated from fitting the adsorption of AY3 (A) and ATL (B) to the Langmuir isotherm model.

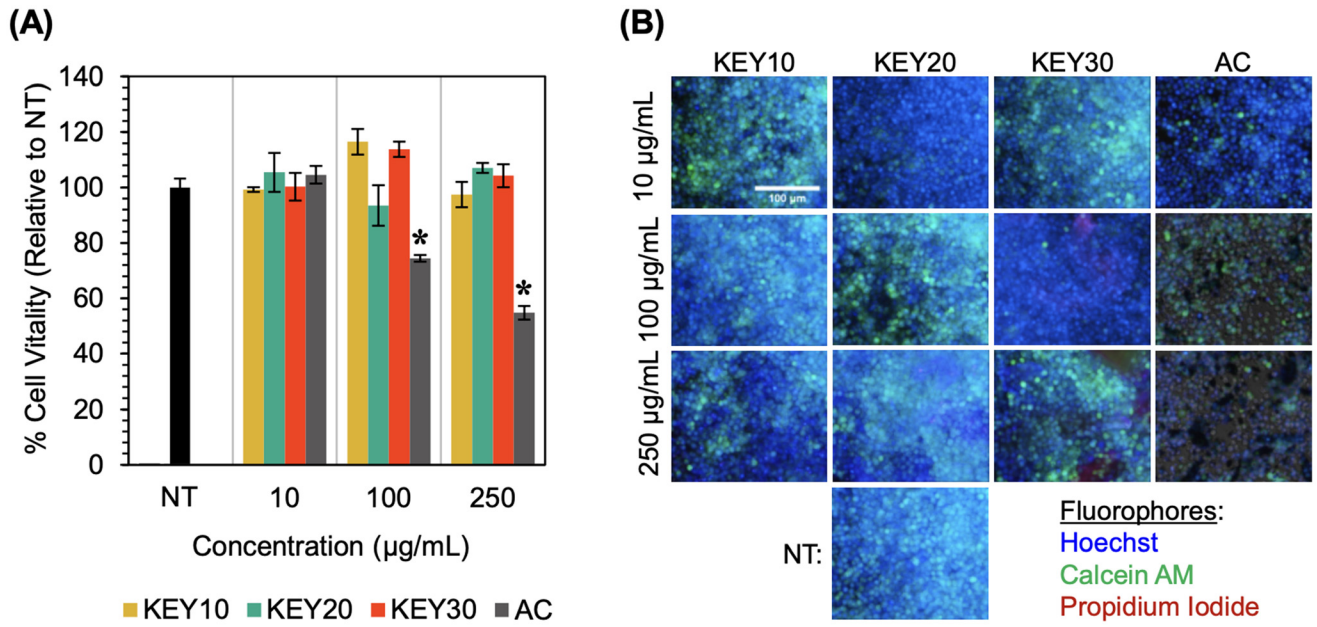

Fig. 8 The *in vitro* cytocompatibility of the KEYs and AC were evaluated with RAW 264.7 macrophages. (A) Cellular vitality was computed from cell counts and reported relative to the "no treatment" condition (NT). The asterisk (*) indicates statistical significance from the NT condition ($p < 0.05$). (B) Representative cell images after exposure to the treatment and NT conditions. Here, fluorescent dyes were used to characterize cytocompatibility: Hoechst (blue) stains cell nuclei, Calcein AM (green) stains the cytoplasm when healthy metabolism is occurring, and propidium iodide (red) stains dying cells. It should be noted that the red/pink crystalline structures in the KEY30 images are attributed to residual KEY30 aggregates, which bind to the propidium iodide dye. The scale bar in the top left image is 100 μm.

at all concentrations. Notably, the images feature numerous, blue- and green-stained cells – indicating healthy, living cells – and there is no red staining (dead cells). Some crystalline, red structures can be observed in the KEY30 images, but this is a result of residual KEY30 aggregates which bind the red propidium iodide stain. At the 250 μg mL^{-1} concentration of AC, poor cell vitality and declining cell health are evident in the relative lack of blue- and green-stained cells and the presence of red-stained cells. Overall, all three KEYs showed significantly better cytocompatibility than activated charcoal.

4. Conclusions

In this work, a class of polypeptide amphiphiles, termed "KEYs", were prepared using NCA ROP and evaluated (*in vitro*) as a treatment option for gastrointestinal decontamination following a drug overdose. Due to their rationally designed amino acid composition, the KEYs form aggregates in aqueous solution that are capable of physically adsorbing and sequestering drug model compounds ("adsorbates") from simulated body fluids. This performance was then evaluated and compared to the clinical standard for gastrointestinal decontamination, activated charcoal (AC). The KEYs were found to adsorb the compounds as rapidly as AC in simulated gastric and intestinal fluids as well as phosphate buffered saline. The adsorption capacity of the KEYs was dependent on their amino acid composition, the pH of the media, and the identity of the adsorbate, however, adsorption appeared to be limited by the low surface area of the KEY aggregates relative to AC. Nevertheless, this study provides proof of concept for the adsorption of drugs to polypeptides. Additionally, these results offer insight into how the molecular architecture and amino acid composition of future generations of polypeptide-based adsorbents could achieve high-capacity and drug-specific adsorption.

The results of this study demonstrate two important areas of improvement that could be implemented in the design of future generations of polypeptide-based adsorbents: (1) the surface area of the polypeptide aggregates should be increased to allow greater contact between the adsorbate and adsorbents and (2) the electrostatic characteristics of the polypeptide-based adsorbents can be tuned to target adsorption of specific drugs in certain pH conditions based on pK_a.

Given the highly adaptable nature of the NCA ROP, this synthetic strategy offers a promising platform for the development of rationally designed, drug-specific polypeptide-based adsorbents that can be used for gastrointestinal decontamination. To this end, development of a safe and effective gastrointestinal decontamination strategy would expand the treatment options for drug overdose patients (including overdose cases that have an antidote) by preventing adsorption of the overdosed drug, thereby decreasing morbidity and mortality.

Author contributions

Karoline Eckhart, Hunter Wood, and Tarik Taoufik contributed equally to the synthesis, characterization, adsorption

studies, and manuscript preparation. Michelle Wolf performed the cytocompatibility studies. Dazhe Cao provided professional toxicologist expertise to guide the development of KEY polypeptides and secured funding. Stefanie Sydlik supervised research and secured funding.

Conflicts of interest

There are no conflicts to declare.

Acknowledgements

For providing use of their facilities, we thank Roberto Gil (NMR, funded in part by NSF grant # CHE-9808188, CHE-1039870, and CHE-1726525), Marcel Bruchez (microplate reader and microcentrifuge), and Kris Matyjaszewski (GPC, zeta potential), all at Carnegie Mellon University.

References

1 H. Hedegaard, A. Miniño and M. Warner, *Drug Overdose Deaths in the United States, 1999–2019*, CDC National Center for Health Statistics, Hyattsville, MD, 2020.
2 C. J. Ruhm, *Health Affairs*, 2019, **38**, 1216–1224.
3 B. L. Hanson, R. R. Porter, A. L. Zöld and H. Terhorst-Miller, *Harm Reduct. J.*, 2020, **17**, 4.
4 L. Enteen, J. Bauer, R. McLean, E. Wheeler, E. Huriaux, A. H. Kral and J. D. Bamberger, *J. Urban Health*, 2010, **87**, 931–941.
5 T. Zellner, D. Prasa, E. Färber, P. Hoffmann-Walbeck, D. Genser and F. Eyer, *Dtsch. Arztebl. Int.*, 2019, **116**, 311–317.
6 H. N. Tran, Y.-F. Wang, S.-J. You and H.-P. Chao, *Process Saf. Environ. Prot.*, 2017, **107**, 168–180.
7 B. Peng, L. Chen, C. Que, K. Yang, F. Deng, X. Deng, G. Shi, G. Xu and M. Wu, *Sci. Rep.*, 2016, **6**, 31920.
8 A. Kumar and H. M. Jena, *Results Phys.*, 2016, **6**, 651–658.
9 K. Ukanwa, K. Patchigolla, R. Sakrabani, E. Anthony and S. Mandavgane, *Sustainability*, 2019, **11**, 6204.
10 J. Saleem, U. B. Shahid, M. Hijab, H. Mackey and G. McKay, *Biomass Convers. Biorefin.*, 2019, **9**, 775–802.
11 D. N. Juurlink, *Br. J. Clin. Pharmacol.*, 2016, **81**, 482–487.
12 L. C. G. Hoegberg, G. Shepherd, D. M. Wood, J. Johnson, R. S. Hoffman, E. M. Caravati, W. L. Chan, S. W. Smith, K. R. Olson and S. Gosselin, *Clin. Toxicol.*, 2021, **59**, 1196–1227.
13 J. Silberman, M. A. Galuska and A. Taylor, in *StatPearls*, StatPearls Publishing, Treasure Island (FL), 2022.
14 R. C. E. Francis, J. C. Schefold, S. Bercker, B. Temmesfeld-Wollbrück, W. Weichert, C. D. Spies and S. Weber-Carstens, *Intensive Care Med.*, 2009, **35**, 360–363.
15 D. Seger, *J. Toxicol., Clin. Toxicol.*, 2004, **42**, 101–110.
16 C. Tomaszewski, *J. Toxicol., Clin. Toxicol.*, 1999, **37**, 17–18.
17 A. De Weerdt, A. Snoeckx, P. Germonpré and P. G. Jorens, *Am. J. Respir. Crit. Care Med.*, 2015, **191**, 344–345.
18 G. R. Graff, J. Stark, J. W. Berkenbosch, G. W. Holcomb and R. E. Garola, *Pediatrics*, 2002, **109**, 959–961.
19 A. Donoso, M. Linares, J. León, G. Rojas, C. Valverde, M. Ramírez and B. Oberpaur, *Pediatr. Emerg. Care*, 2003, **19**, 420–421.
20 D. B. Seder, R. A. Christman, M. O. Quinn and M. E. Knauft, *Respir. Care*, 2006, **51**, 1251–1254.
21 F. R. Justiniani, R. Hippalgaonkar and L. O. Martinez, *Chest*, 1985, **87**, 404–405.
22 C. G. Elliott, T. V. Colby, T. M. Kelly and H. G. Hicks, *Chest*, 1989, **96**, 672–674.
23 K. B. Goulbourne and J. E. Cisek, *Ann. Emerg. Med.*, 1994, **24**, 108–110.
24 H. F. Gomez, J. A. Brent, D. C. Munoz, R. F. Mimmack, J. Ritvo, S. Phillips and P. McKinney, *J. Emerg. Med.*, 1994, **12**, 57–60.
25 C.-J. Lin, C.-Y. Sun, C.-J. Wu, C.-C. Wu, V. Wu and F.-H. Lin, *Int. J. Mol. Sci.*, 2020, **21**, 1257.
26 M. Moosavi, *Iran. J. Public Health*, 2017, **46**, 1176–1183.
27 A. K. Tiwary, R. H. Poppenga and B. Puschner, *Clin. Toxicol.*, 2009, **47**, 213–218.
28 B. K. Olopade, S. U. Oranusi, O. C. Nwinyi, I. A. Lawal, S. Gbashi and P. B. Njobeh, *Toxins*, 2019, **11**, 616.
29 E. Boccaleri, C. Marzetti, G. Celoria, C. Cassino, G. Paul, I. Miletto and E. Gianotti, *Materials*, 2021, **14**, 6196.
30 M. Delle Piane, S. Vaccari, M. Corno and P. Ugliengo, *J. Phys. Chem. A*, 2014, **118**, 5801–5807.
31 S. A. E. Young, J. Muthami, M. Pitcher, P. Antovski, P. Wamea, R. D. Murphy, R. Haghniaz, A. Schmidt, S. Clark, A. Khademhosseini and A. Sheikhi, *Mater. Today Chem.*, 2022, **23**, 100711.
32 H. Yang, A. Sheikhi and T. G. M. van de Ven, *Langmuir*, 2016, **32**, 11771–11779.
33 M. Tavakolian, H. Wiebe, M. A. Sadeghi and T. G. M. van de Ven, *ACS Appl. Mater. Interfaces*, 2020, **12**(1), 73.
34 C. M. Blumenfeld, M. D. Schulz, M. S. Aboian, M. W. Wilson, T. Moore, S. W. Hetts and R. H. Grubbs, *Nat. Commun.*, 2018, **9**, 2870.
35 D. W. Yee, S. W. Hetts and J. R. Greer, *ACS Appl. Mater. Interfaces*, 2021, **13**, 41424–41434.
36 A. S. Patel, M. Saeed, E. J. Yee, J. Yang, G. J. Lam, A. D. Losey, P. V. Lillaney, B. Thorne, A. K. Chin, S. Malik, M. W. Wilson, X. C. Chen, N. P. Balsara and S. W. Hetts, *J. Med. Device*, 2014, **8**(4), 0410081–0410088.
37 H. J. Oh, M. S. Aboian, M. Y. J. Yi, J. A. Maslyn, W. S. Loo, X. Jiang, D. Y. Parkinson, M. W. Wilson, T. Moore, C. R. Yee, G. R. Robbins, F. M. Barth, J. M. DeSimone, S. W. Hetts and N. P. Balsara, *ACS Cent. Sci.*, 2019, **5**, 419–427.
38 X. C. Chen, H. J. Oh, J. F. Yu, J. K. Yang, N. Petzetakis, A. S. Patel, S. W. Hetts and N. P. Balsara, *ACS Macro Lett.*, 2016, **5**, 936–941.
39 J. Cappello, *Trends Biotechnol.*, 1990, **8**, 309–311.
40 A. Varanko, S. Saha and A. Chilkoti, *Adv. Drug Delivery Rev.*, 2020, **156**, 133–187.

41 D. Chow, M. L. Nunalee, D. W. Lim, A. J. Simnick and A. Chilkoti, *Mater. Sci. Eng., R*, 2008, **62**, 125–155.
42 A. Chilkoti, M. R. Dreher and D. E. Meyer, *Adv. Drug Delivery Rev.*, 2002, **54**, 1093–1111.
43 L. I. Atanase, *Polymers*, 2021, **13**, 477.
44 C. Ziemba, M. Khavkin, D. Priftis, H. Acar, J. Mao, M. Benami, M. Gottlieb, M. Tirrell, Y. Kaufman and M. Herzberg, *Langmuir*, 2019, **35**, 1699–1713.
45 Y.-C. Huang, Y.-S. Yang, T.-Y. Lai and J.-S. Jan, *Polymer*, 2012, **53**, 913–922.
46 C. A. Rey-Mafull, J. E. Tacoronte, R. Garcia, J. Tobella, J. C. Llópiz, A. Iglesias and D. Hotza, *SpringerPlus*, 2014, **3**, 48.
47 E. Stippler, S. Kopp and J. B. Dressman, *Dissolution Technol.*, 2004, **11**, 6–10.
48 M. Zelzer and A. Heise, *Polym. Chem.*, 2013, **4**, 3896.
49 D. Maurya, R. Nisal, R. Ghosh, P. Kambale, M. Malhotra and M. Jayakannan, *Eur. Polym. J.*, 2023, **183**, 111754.
50 Y. Han, W. Wang, Y. Tang, S. Zhang, Z. Li and Y. Wang, *Langmuir*, 2013, **29**, 9316–9323.
51 C.-H. Luan, T. M. Parker, D. C. Gowda and D. W. Urry, *Biopolymers*, 1992, **32**, 1251–1261.
52 G. B. McGaughey, M. Gagné and A. K. Rappé, *J. Biol. Chem.*, 1998, **273**, 15458–15463.
53 A. T. Cartus, in *Chemical Contaminants and Residues in Food*, ed. D. Schrenk, Woodhead Publishing, 2012, pp. 286–319.
54 G. Zhang and H. J. Sun, *PLoS One*, 2014, **9**, e92101.
55 D. V. Grishin, D. D. Zhdanov, M. V. Pokrovskaya and N. N. Sokolov, *All Life*, 2020, **13**, 11–22.
56 M. Deptuła, A. Wardowska, M. Dzierżyńska, S. Rodziewicz-Motowidło and M. Pikuła, *Molecules*, 2018, **23**, 414.
57 L.-Y. Zhou, Y.-H. Zhu, X.-Y. Wang, C. Shen, X.-W. Wei, T. Xu and Z.-Y. He, *Comput. Struct. Biotechnol. J.*, 2020, **18**, 1980–1999.
58 E. J. Liu, A. Sinclair, A. J. Keefe, B. L. Nannenga, B. L. Coyle, F. Baneyx and S. Jiang, *Biomacromolecules*, 2015, **16**, 3357–3361.
59 A. D. White, A. K. Nowinski, W. Huang, A. J. Keefe, F. Sun and S. Jiang, *Chem. Sci.*, 2012, **3**, 3488.
60 S. Chen, Z. Cao and S. Jiang, *Biomaterials*, 2009, **30**, 5892–5896.
61 A. K. Nowinski, F. Sun, A. D. White, A. J. Keefe and S. Jiang, *J. Am. Chem. Soc.*, 2012, **134**, 6000–6005.
62 S. Banskota, P. Yousefpour, N. Kirmani, X. Li and A. Chilkoti, *Biomaterials*, 2019, **192**, 475–485.
63 Y. Shalitin and E. Katchalski, *J. Am. Chem. Soc.*, 1960, **82**, 1630–1636.
64 G. Liu, X. Hu, C. Chen, Q. Jin and J. Ji, *Polym. Int.*, 2011, **60**, 578–583.
65 X.-H. Dai and C.-M. Dong, *J. Polym. Sci., Part A: Polym. Chem.*, 2008, **46**, 817–829.
66 P. K. Das, D. N. Dean, A. L. Fogel, F. Liu, B. A. Abel, C. L. McCormick, E. Kharlampieva, V. Rangachari and S. E. Morgan, *Biomacromolecules*, 2017, **18**, 3359–3366.
67 Y. Z. Liang, Z. C. Li and F. M. Li, *J. Colloid Interface Sci.*, 2000, **224**, 84–90.
68 D. Balasubramanian, B. Raman and C. S. Sundari, *J. Am. Chem. Soc.*, 1993, **115**, 74–77.
69 F. M. Winnik, *Macromolecules*, 1989, **22**, 734–742.
70 D. Huesmann, A. Birke, K. Klinker, S. Türk, H. J. Räder and M. Barz, *Macromolecules*, 2014, **47**, 928–936.
71 D. Huesmann, A. Sevenich, B. Weber and M. Barz, *Polymer*, 2015, **67**, 240–248.
72 G. V. Lowry, R. J. Hill, S. Harper, A. F. Rawle, C. Ogilvie Hendren, F. Klaessig, U. Nobbmann, P. Sayre and J. Rumble, *Environ. Sci.: Nano*, 2016, **3**, 953–965.
73 H.-K. Tsao, *J. Colloid Interface Sci.*, 2000, **225**, 247–250.
74 B. Cohen, D. Huppert and N. Agmon, *J. Am. Chem. Soc.*, 2000, **122**, 9838–9839.
75 M. Takahashi, *J. Phys. Chem. B*, 2005, **109**, 21858–21864.
76 X. Yao, A. L. Neusaenger and L. Yu, *Pharmaceutics*, 2021, **13**, 1271.
77 V. Kholodovych and W. J. Welsh, in *Physical Properties of Polymers Handbook*, ed. J. E. Mark, Springer New York, New York, NY, 2007, pp. 611–617.
78 I. Douglass and P. Harrowell, *J. Phys. Chem. B*, 2018, **122**, 2425–2433.
79 J. Yang, X. Zhen, B. Wang, X. Gao, Z. Ren, J. Wang, Y. Xie, J. Li, Q. Peng, K. Pu and Z. Li, *Nat. Commun.*, 2018, **9**, 840.
80 S. E. Wheeler, *Acc. Chem. Res.*, 2013, **46**, 1029–1038.
81 C. A. Hunter and J. K. M. Sanders, *J. Am. Chem. Soc.*, 1990, **112**, 5525–5534.
82 P. I. Dargan, M. G. Colbridge and A. L. Jones, *Toxicol. Rev.*, 2005, **24**, 187–194.
83 J. Silberman, M. A. Galuska and A. Taylor, *Activated Charcoal*, StatPearls Publishing, Treasure Island, FL, 2022.
84 Z. Wu, X. Ye, H. Liu, H. Zhang, Z. Liu, M. Guo, Q. Li and J. Li, *Pure Appl. Chem.*, 2020, **92**, 1655–1662.
85 C. A. Rey-Mafull, J. E. Tacoronte, R. Garcia, J. Tobella, J. C. Llópiz, A. Iglesias and D. Hotza, *SpringerPlus*, 2014, **3**, 48.
86 V. C. Srivastava, M. M. Swamy, I. D. Mall, B. Prasad and I. M. Mishra, *Colloids Surf., A*, 2006, **272**, 89–104.
87 L. Largitte and R. Pasquier, *Chem. Eng. Res. Des.*, 2016, **109**, 495–504.
88 A. Malek and S. Farooq, *AIChE J.*, 1996, **42**, 3191–3201.
89 F. Ali, N. Ali, I. Bibi, A. Said, S. Nawaz, Z. Ali, S. M. Salman, H. M. N. Iqbal and M. Bilal, *Case Stud. Chem. Environ. Eng.*, 2020, **2**, 100040.
90 B. Subramanyam and A. Das, *J. Environ. Health Sci. Eng.*, 2014, **12**, 92.
91 N. Ayawei, A. N. Ebelegi and D. Wankasi, *J. Chem.*, 2017, **2017**, e3039817.
92 S. Guha, T. Chakraborty and A. Banerjee, *Green Chem.*, 2009, **11**, 1139–1145.
93 P. D. Sarvalkar, A. S. Vadanagekar, O. S. Karvekar, P. D. Kumbhar, S. S. Terdale, A. S. Thounaojam, S. S. Kolekar, R. S. Vhatkar, P. S. Patil and K. K. K. Sharma, *ACS Omega*, 2023, **31**(14), 13285–13299.
94 T. K. Aljohani, A. M. Alshamrani, A. M. Alzahrani and R. A. Sairafi, *J. Surg. Case Rep.*, 2019, **2019**, rjz033.
95 J. A. Lowry, *Use of Activated Charcoal in Pediatric Populations*, Division of Clinical Pharmacology and Medical Toxicology, Geneva, 2008.